

A CONVOLUTIONAL RIEMANNIAN TEXTURE MODEL WITH DIFFERENTIAL ENTROPIC ACTIVE CONTOURS FOR UNSUPERVISED PEST DETECTION

Shuanglu Dai and Hong Man

Department of Electrical and Computer Engineering,
Stevens Institute of Technology,
1 Castle Point on Hudson, Hoboken, NJ07030, U.S.A.

sdail@stevens.edu, hong.man@stevens.edu

ABSTRACT

Pest camouflages in grains or natural environment cause significant difficulties in pest detection using imaging technologies. This paper proposes a convolutional Riemannian texture with differential entropic active contours to distinguish the background regions and expose pest regions. An image texture model is firstly introduced on the Riemannian manifold. A convolutional Riemannian texture structure is then explored to reduce the environmental background textures and highlight potential pest textures. Subsequently, a differential entropic active contour model is developed to estimate the foreground and background distributions. Finally, the estimated foreground and background distributions are used to distinguish pest textures and environmental textures. The final detected regions are obtained by maximizing pixel-wise posterior probabilities on the estimated distributions. Experimental results show that effective detections can be achieved by the proposed method on forestry pests imaging datasets.

Index Terms— Unsupervised pest detection; Riemannian texture; Active Contours

1. INTRODUCTION

Effective pest detection and control can increase food security, improve the quality of life and reduce the cost in agriculture. Pest images usually consist of some static environmental background with pests as outliers. With such prior information, it is possible to design an unsupervised method for image-based pests detection.

Pest detection methods can be mainly divided into two categories: sensor-based and camera-based. Sensor-based methods mainly rely on sensor technologies specially designed according to pest living habits. In order to detect the sub-populations of invasive species, Homans et al. proposed an optimal detection strategy by dividing the uninfested landscape into suppression zone and an eradication zone [1]. Ferro et al. designed a wireless sensor network with photoelectric sensors for early snail pest detection and control [2]. Although effective, sensor-based methods are mostly applied

to specific spices and living environments. Different spices usually require different sensors and methods [2].

In recent years, many computer vision methods have been used for camera-based pest detection. Fina et al. proposed to learn correspondence filters with k-means clustering to detect and recognize pests. Mostafa et al. proposed a histogram adjustment method with a Gabor filter to improve the texture-based plant disease recognition[3]. In order to detect pests in greenhouse crops, Paul et al. proposed a cognitive vision approach using ontology based object recognition[4, 5]. Vision techniques adopted by environmental specialists are often computationally expensive with complicated processes. However, pest images frequently contain stable texture backgrounds and pests usually appear to be outliers. It is thus possible to have an unsupervised framework for efficient pest detection.

This paper proposes a convolutional Riemannian texture with geodesic priors to model the pest target and environmental background in common pest images. Inspired by the idea of texture analysis, pests are segmented as texture outliers in the environment[6, 7, 8]. Firstly, an object enhanced texture model is introduced on the Riemannian manifold. Secondly, a convolutional structure is explored to reduce the background texture and expose the pest texture. Then a probabilistic texture image model is developed. Target regions and background regions are modelled by foreground and background distributions respectively. Finally, a symmetric differential entropy is introduced to measure the distance of these two distributions and to derive the resulting active contours. Promising results obtained on forestry pests imaging datasets demonstrate the effectiveness of the proposed method.

2. SEMI-LOCAL RIEMANNIAN TEXTURE BASED ON BELTRAMI FRAMEWORK

Introduced by Sochen, Kimmel and Malladi in[9], Beltrami representation is a typical local image texture representation. The geometric representation of images considers a standard 2-dimensional gray-value image function $I(x, y)$ as a mapping $I : R^2 \rightarrow R$. Assuming the independency of the

local pixels, function I of local coordinates (x, y) can be embedded on a surface by a mapping F from R^2 to R^3 where $F : (x, y) \rightarrow (x, y, I(x, y))$ [7, 10, 11, 12]. A k -vector image $I_k(x, y)$ can be described as a k -dimension manifold embedding to a $(k + 2)$ -dimensional space with the mapping $F : (x, y) \rightarrow (x, y, I_1(x, y), I_2(x, y), \dots, I_k(x, y))$. The first fundamental form, which is also called metric tensor[13, 14], is computed as $g_{uv} = \langle \frac{\partial M}{\partial u}, \frac{\partial M}{\partial v} \rangle$ where u, v are two orthogonal directions on the embedding Riemannian Manifold $M_{I(x, y)}$. Since $\{x, y\} \in \{u, v\}$, one of the explicit first fundamental form on the manifold M can be written as

$$g_{xy} = \begin{pmatrix} g_{xx} & g_{xy} \\ g_{yx} & g_{yy} \end{pmatrix} = \begin{pmatrix} 1 + I_x^2 & I_x I_y \\ I_x I_y & 1 + I_y^2 \end{pmatrix} \quad (1)$$

where its suffix is in form of an edge detector operating on the functional space $I(x, y)$: $\frac{1}{\det(g_{xy})} = \frac{1}{1 + |\nabla I(x, y)|^2}$ where $\nabla(\cdot)$ is the gradient operator, $\det(\cdot)$ is the determinant operator, and $|\cdot|$ is the norm operator. The edge detector function shows the local texture of an image but it is sensitive to noise. In order to have a texture representation that is robust to noise, Houhou et al. proposed a semi-local Riemannian texture descriptor[15]. Let $P(I(x, y))$ denote a $\tau \times \tau$ square patch function around (x, y) :

$$P(I(x, y)) = \{I(x + t_x, y + t_y)\}, t_x \in [-\frac{\tau}{2}, \frac{\tau}{2}], t_y \in [-\frac{\tau}{2}, \frac{\tau}{2}] \quad (2)$$

$P(I(x, y))$ is a semi-local patch function of (x, y) when $\tau > 1$. The representation follows the mapping: $(x, y) \rightarrow (x, y, I(x, y)) \rightarrow (x, y, P(I(x, y)))$ where $P(I(x, y))$ lies on a manifold with surface $(x, y, P(I(x, y)))$. Its metric tensor is computed as

$$g_{xy} = \begin{pmatrix} 1 + [\partial_x P(I(x, y))]^2 & \partial_x P(I(x, y)) \partial_y P(I(x, y)) \\ \partial_x P(I(x, y)) \partial_y P(I(x, y)) & 1 + [\partial_y P(I(x, y))]^2 \end{pmatrix} \quad (3)$$

The semi-local intrinsic texture descriptor can be designed similarly as the edge detector with a Gaussian kernel: $K_{\sigma, \tau}(x, y) = \exp(-\frac{\det(g_{xy})}{\sigma^2})$ For a k -vector valued image, the representation follows the mapping: $(x, y) \rightarrow (x, y, I_1(x, y), I_2(x, y), \dots, I_k(x, y)) \rightarrow (x, y, P(I_1(x, y)), P(I_2(x, y)), \dots, P(I_k(x, y)))$. Its metric tensor is derived as

$$g_{xy} = \begin{pmatrix} 1 + \sum_{j=1}^k [\partial_x P(I_j(x, y))]^2 & \sum_{j=1}^k \partial_x P(I_j(x, y)) \partial_y P(I_j(x, y)) \\ \sum_{j=1}^k \partial_x P(I_j(x, y)) \partial_y P(I_j(x, y)) & 1 + \sum_{j=1}^k [\partial_y P(I_j(x, y))]^2 \end{pmatrix} \quad (4)$$

The intrinsic texture descriptor computed by $K_{\tau, \sigma}(x, y)$ is robust to noise by considering gradient information in the semi-local patch function.

3. CONVOLUTIONAL RIEMANNIAN TEXTURE MODEL

Large size of patches in the semi-local patch function can enhance textures in the semi-local regions, but they may ignore local regions. When $\tau = 1$, the edge detector function is equivalent to the semi-local texture. In this work we introduce a novel convolutional Riemannian texture model to highlight pest regions from the environmental background regions.

Two conditions make the proposed convolutional structure possible. Firstly, the determinant of the metric tensor in $K_{\tau, \sigma}(x, y)$ can be considered as a convolution of g_{xy}

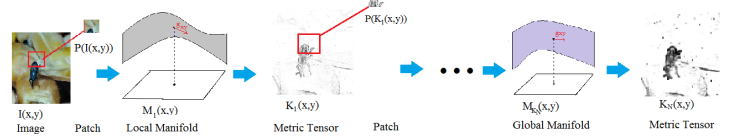


Fig. 1. Mapping structure illustrating the convolutional Riemannian texture. Image function is sampled by a semi-local patch function. Metric tensor is computed on the local Riemannian manifold with a Gaussian kernel. The patches and convolutional kernels are computed several times with different patch sizes to generate global texture.

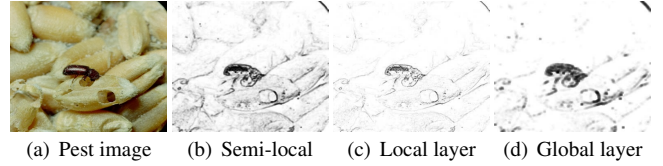


Fig. 2. An instance of the proposed texture model compared with the semi-local texture descriptor proposed by Houhou et al.[8]

with a kernel $D^{\tau \times \tau}$, where $K_{\sigma}(x, y) = \exp(\frac{g_{xy} * D}{\sigma^2})$; $*$ denotes the convolution operator. Secondly, the kernel operation in $K_{\tau, \sigma}(x, y)$ embeds semi-local image patches into a new manifold $M_{K_{\tau, \sigma}(x, y)}$ with surface $(x, y, K_{\tau, \sigma}(x, y))$, where $(x, y) \in R^2$ and $K_{\tau, \sigma}(x, y) \in R$. The convolutional structures can be considered as iteratively mapping from manifold to manifold:

$$M_I(x, y) \rightarrow M_{1, K_{\tau_1, \sigma_1}(x, y)} \rightarrow M_{2, K_{\tau_2, \sigma_2}(x, y)} \dots \rightarrow M_{N, K_{\tau_N, \sigma_N}(x, y)} \quad (5)$$

Figure 1 demonstrates the mapping structure of the proposed convolutional Riemannian texture model.

Let $M_i, i \in [1, N]$ denote the i -th manifold, its metric tensor and descriptor function can be computed as

$$g_{i, xy} = \begin{pmatrix} 1 + [\partial_x P(K_{\sigma_i, \tau_i}(x, y))]^2 & \partial_x P(K_{\sigma_i, \tau_i}(x, y)) \partial_y P(K_{\sigma_i, \tau_i}(x, y)) \\ \partial_x P(K_{\sigma_i, \tau_i}(x, y)) \partial_y P(K_{\sigma_i, \tau_i}(x, y)) & 1 + [\partial_y P(K_{\sigma_i, \tau_i}(x, y))]^2 \end{pmatrix} \quad (6)$$

where $\tau_i, \sigma_i, i \in [1, N]$ denote the i -th patch size and kernel parameter, respectively; $K_{\sigma_{i+1}, \tau_{i+1}}(x, y) = \exp(-\frac{\det(g_{i, xy})}{\sigma_i^2})$.

Figure 2 shows an instance of the proposed texture model compared with the semi-local texture descriptor proposed by Houhou et al.[8]. One can observe that local textures are kept by the local layer with $\tau = 3$ and the global layers further reduce the background texture and expose the pest texture with a semi-local layer at $\tau = 8$. The final output from the global layer reduces the background textures and exposes the pest texture to certain extent. But the semi-local texture descriptor is not able to reduce the background textures. The patch sizes of semi-local texture descriptor for each image need to be set empirically for better performance. Differently, the patch sizes τ and kernel bandwidth σ of the proposed methods are the same under similar environments.

4. DIFFERENTIAL ENTROPIC ACTIVE CONTOURS

Given the proposed texture with enhanced objects and reduced background, the object regions are still impossible to be located by simple thresholds. A distribution-based active contour is thus adopted for the detection. Consider a closed parameterized planar curve, $C(v, t) : [0, 1) \times [0, \infty) \rightarrow R^2$ where

v is the planar directional vector and $t \in [0, \infty)$ is the temporal variable[16]. Define a bounded variational function domain $BV(\Omega) = \{u \in L^1(\Omega) : \int_{\Omega} |Du| < \infty\}$ where $L^1(\cdot)$ denotes a set of functions with first-order lower semi-continuity; $|Du|$ is the Lebesgue measure. Let ϕ be a level set function of C : $C(v, t) = \{x | C \in \Omega, \phi(x, t) = 0, \phi \in BV(\Omega)\}$, where $\phi \in [0, 1]$ is with the same definition as a probability density function(pdf). It is obvious that the pixel location $x \in \Omega$, the image function $I(x) \in BV(\Omega)$ and the Riemannian texture function $K(x) \in BV(\Omega)$.

The goal of the proposed active contour method is to find an optimized pdf $\phi(x)$. Its zero level set gives a background/foreground probabilistic boundary. Given texture function $K(x), x \in \Omega$, the background and foreground probability functions can be defined as

$$\begin{cases} p_f(\widehat{K}(x), \Omega) = \frac{1}{|\Omega_f|} \int_{\Omega_f} G_{\sigma}(\widehat{K}(x) - K(x)) dx \\ p_b(\widehat{K}(x), \Omega) = \frac{1}{|\Omega_b|} \int_{\Omega_b} G_{\sigma}(\widehat{K}(x) - K(x)) dx \end{cases} \quad (7)$$

where p_f and p_b are foreground and background pdfs, respectively; K is the observed texture function, \widehat{K} is the signed distance function indicating distances to the zero level set; G_{σ} is a Gaussian kernel; Ω indicates the texture image domain; Ω_b indicates the image background and Ω_f indicates the image foreground where $\Omega \setminus \Omega_f = \Omega_b, \Omega \setminus \Omega_b = \Omega_f$; $|\cdot|$ computes the area of a given region. Here we introduce a symmetric differential entropy as a distance measure that measures the difference between the foreground and background pdfs.

$$D(\Omega) = \int_{R^+} p_f(\widehat{K}, \Omega) \log \frac{p_f(\widehat{K}, \Omega)}{p_b(\widehat{K}, \Omega)} + p_b(\widehat{K}, \Omega) \log \frac{p_b(\widehat{K}, \Omega)}{p_f(\widehat{K}, \Omega)} d\widehat{K} \quad (8)$$

The goal is to maximize the differential entropy between p_b and p_f w.r.t. set Ω . According to the Radon-Nikodym theorem, the integration along boundary direction between Ω_b and Ω_f should be considered in a Lebesgue integration, which is the length of the closed contour C [17]: $L(\Omega) = \int_{\partial\Omega} dv$. Together with Eq.(8), the objective function is written as

$$E(\Omega) = D(\Omega) + \lambda L(\Omega) \quad (9)$$

where v is the directional unit of the planar curve C , $\lambda > 0$ is a parameter. The optimization problem is to find the maximized energy w.r.t. a set separation of Ω : $\max_{\Omega_b, \Omega_f} E(\Omega)$. Introduce a characteristic function for all the elements $x \in \Omega$:

$$\Psi_{\Omega_f}(x) = \begin{cases} 1, x \in \Omega_f \\ 0, x \in \Omega \setminus \Omega_f \end{cases}, \Psi_{\Omega_b}(x) = 1 - \Psi_{\Omega_f}(x) = \begin{cases} 1, x \in \Omega_b \\ 0, x \in \Omega \setminus \Omega_b \end{cases} \quad (10)$$

The area of the set $|\Omega_b| = \int_{\Omega} \Psi_{\Omega_b}(x) dx, |\Omega_f| = \int_{\Omega} \Psi_{\Omega_f}(x) dx$. The foreground and background pdf can be re-written as the following form:

$$\begin{cases} p_f(\widehat{K}(x), \Psi_{\Omega_f}(x), \Psi_{\Omega_b}(x)) = \frac{\int_{\Omega} G_{\sigma}(\widehat{K}(x) - K(x)) \Psi_{\Omega_f}(x) dx}{\int_{\Omega} \Psi_{\Omega_f}(x) dx} \\ p_b(\widehat{K}(x), \Psi_{\Omega_f}(x), \Psi_{\Omega_b}(x)) = \frac{\int_{\Omega} G_{\sigma}(\widehat{K}(x) - K(x)) \Psi_{\Omega_b}(x) dx}{\int_{\Omega} \Psi_{\Omega_b}(x) dx} \end{cases} \quad (11)$$

The length function $L(\Omega)$ can be re-written as:

$$L(\Psi_{\Omega_f}(x), \Psi_{\Omega_b}(x)) = \int_{\Omega} |\nabla \Psi_{\Omega_f}(x)| dx \quad (12)$$

Note that the integration follows the pixel direction x by embedding the characteristic function. The objective function becomes

$$E(\Psi_{\Omega_f}, \Psi_{\Omega_b}) = D(\Psi_{\Omega_f}, \Psi_{\Omega_b}) + \lambda L(\Psi_{\Omega_f}, \Psi_{\Omega_b}) \quad (13)$$

The optimization in Eq.(13) shares a similar form with the KL-divergence based active contour model proposed in [15]. Let $u(x) = \Psi_{\Omega_f}(x)$, the speed V_D provided by the differential entropy in the normal inward direction is computed by

$$\begin{aligned} V_D = \int_{R^+} \frac{1}{\int_{\Omega} u dx} \left[1 - \frac{p_f(u)}{p_b(u)} + \log \frac{p_b(u)}{p_f(u)} \right] \cdot [G_{\sigma}(\widehat{K} - K - p_f(u))] d\widehat{K} \\ + \int_{R^+} \frac{1}{\int_{\Omega} (1-u) dx} \left[1 - \frac{p_f(u)}{p_b(u)} + \log \frac{p_b(u)}{p_f(u)} \right] \cdot [-G_{\sigma}(\widehat{K} - K) + p_b(u)] d\widehat{K} \end{aligned} \quad (14)$$

The optimization problem can be simplified as

$$\min_u \int_{\Omega} -\lambda V_D u + |\nabla u|, \quad (15)$$

Eq.(15) can be solved with split Bregman method by adding a constraint $d = \nabla u$ and an inference variable m to de-couple variable u :

$$\begin{cases} (u^{k+1}, d^{k+1}) = \min_{0 \leq u \leq 1, d} \|d\| + \lambda V_D u + \frac{\beta}{2} \|d - \nabla u - m^k\|_2^2 \\ m^{k+1} = m^k + \nabla u^{k+1} - d^{k+1} \end{cases} \quad (16)$$

The Euler-Lagrangian equation is

$$\beta \Delta u = \lambda V_D + \beta \text{div}(d^k - b^k) \quad (17)$$

The solution of (u, d) given by Gauss-Seidel method is

$$\begin{aligned} \gamma_{i,j} = \frac{1}{4} [u_{i-1,j}^k + u_{i+1,j}^k + u_{i,j-1}^k + u_{i,j+1}^k - \frac{\lambda}{\beta} V_D + (b_{i,j}^k - b_{i-1,j}^k + b_{i,j}^k - b_{i,j-1}^k \\ - d_{i,j}^k - d_{i-1,j}^k + d_{i,j}^k - d_{i,j-1}^k)], u_{i,j}^{k+1} = \max\{\min\{\gamma_{i,j}, 1\}, 0\} \end{aligned} \quad (18)$$

$$d^{k+1} = \text{sgn}(\nabla u^{k+1} + b^k) \max\{|\nabla u^{k+1} + b^k| - \lambda^{-1}, 0\} \quad (19)$$

where (i, j) is the pixel position.

5. EXPERIMENTAL RESULTS

Experiments are designed to compare the proposed method with two object proposal methods and a texture segmentation method on pest detection. Algorithms are running on Intel(R) Core(TM) i5-4200M CPU @ 2.5GHz 2.5GHz with 8GB RAM (7.67GB usage) and 64bit OS. The three comparative methods are: Fast texture segmentation based on semi-local texture descriptor proposed in [8]; Category Independent Object Proposals (CIOP) proposed in [18] and Geodesic Object Proposals (GOP) proposed in [19]. Pest images are obtained from forestry images database [20].

“Forestry images” is an ongoing project supported by the USDA Forest Service, Forest Health Technology Enterprise Team and Washington Office, Forest Health Protection Staff. ForestryImages.org utilizes a fully searchable, relational database-driven system to track and provide scientific, descriptive and photographic credit information. Over 4,500 photographs and other images of more than 800 insects, diseases, plants, wildlife, and management practices taken by over 170 photographers are available. Images were digitized

Table 1. Accuracies(%) obtained by the proposed method and the comparative methods.

Methods	Detected	Detected with extra regions
CIOP[18]	64.06	57.81
GOP[19]	55.89	19.12
Semi-local[8]	75.76	37.87
Proposed	89.39	19.69

Table 2. Mean and standard deviation of the computational times (secs) obtained by the proposed method and the comparative methods.

Methods	CIOP[18]	GOP[19]	Semi-local[8]	Proposed
Times	80.65±66.91	15.21±4.12	1.81±0.74	1.31±0.47

from high-resolution 35mm slides. 200 stored food pest images with various environmental backgrounds are used as test images. Pests in the experimental images are often with camouflage colors and partial occlusions.

Some examples of the detection results from the comparative methods and the proposed method are shown in Figure 3. Note that the forth image shows two pests, one with full body and the other with a head. As we can see, the detection results obtained by the proposed method are more accurate and more robust to various environments than those of others.

Furthermore, the performance of the proposed method is evaluated in terms of accuracy. We separate the detection results into 2 types: pest detected and detected with extra regions. The percentage of the two types of results are computed. Table 1 shows that the proposed method achieves highest accuracies with the second least extra regions. GOP achieves the least extra regions but with the lowest accuracies.

Last but not least, computational times of the proposed method are compared with the comparative methods. Both mean and standard deviation of the computational times are shown in Table 2. Figure 4 shows the individual computational times for each of the experimental images. As Table 2 and Figure 4 shows, the proposed method is faster than others. In summary, the proposed method outperforms the comparative methods in terms of accuracy and efficiency in unsupervised pest detection.

6. CONCLUSIONS

This paper proposed a convolutional Riemannian texture model and a differential entropy based active contour method for efficient pest detection in images. Pest targets and environmental backgrounds are modelled by foreground/background distributions. Efficient and accurate detections are achieved by the proposed method. Future work will extend the proposed approach to analyze semantic objects in the nature images.

7. REFERENCES

- [1] F. Homans and T. Horie, "Optimal detection strategies for an established invasive pest," *Ecological economics*, vol. 70, no. 6, pp. 1129–1138, 2011.
- [2] E. Ferro, V. Brea, D. Cabello, P. Lopez, J. Iglesias, and J. Castillejo, "Wireless sensor mote for snail pest detection,"

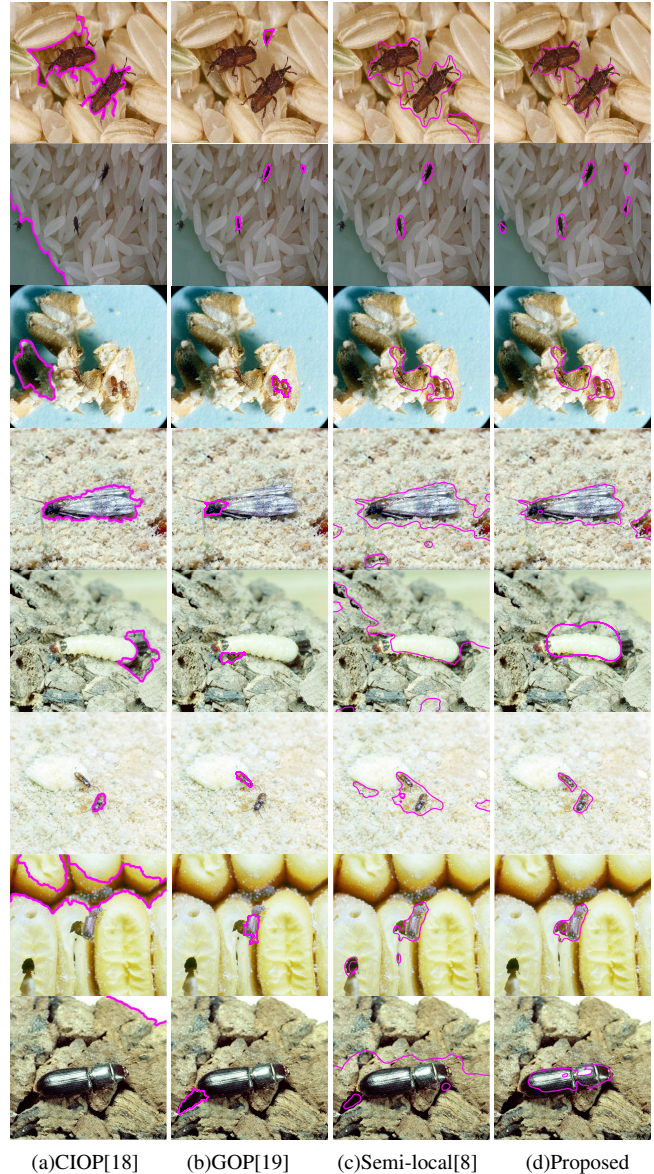


Fig. 3. Example detection results obtained by the comparative methods and the proposed method. The proposed method achieves better detections in various environmental backgrounds.

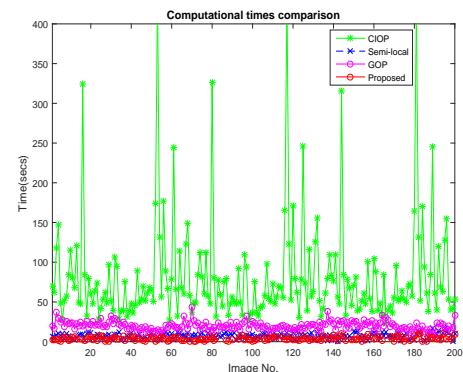


Fig. 4. Comparison of running times.

- in *IEEE SENSORS 2014 Proceedings*. IEEE, 2014, pp. 114–117.
- [3] M. Bayat, M. Abbasi, A. Yosefi *et al.*, “Improvement of pest detection using histogram adjustment method and gabor wavelet,” *Journal of Asian Scientific Research*, vol. 6, no. 2, pp. 24–33, 2016.
- [4] N. E. Maillot and M. Thonnat, “Ontology based complex object recognition,” *Image and Vision Computing*, vol. 26, no. 1, pp. 102–113, 2008.
- [5] P. Boissard, V. Martin, and S. Moisan, “A cognitive vision approach to early pest detection in greenhouse crops,” *computers and electronics in agriculture*, vol. 62, no. 2, pp. 81–93, 2008.
- [6] Q. Ge, L. Xiao, J. Zhang, and Z. H. Wei, “An improved region-based model with local statistical features for image segmentation,” *Pattern Recognition*, vol. 45, no. 4, pp. 1578–1590, 2012.
- [7] C. Sagiv, N. A. Sochen, and Y. Y. Zeevi, “Integrated active contours for texture segmentation,” *IEEE Transactions on image processing*, vol. 1, no. 1, pp. 1–19, 2004.
- [8] N. Houhou, J.-P. Thiran, and X. Bresson, “Fast texture segmentation based on semi-local region descriptor and active contour,” *Numerical Mathematics: Theory, Methods and Applications.*, vol. 2, no. EPFL-ARTICLE-140431, pp. 445–468, 2009.
- [9] N. Sochen, R. Kimmel, and R. Malladi, “A general framework for low level vision,” *IEEE transactions on image processing*, vol. 7, no. 3, pp. 310–318, 1998.
- [10] Q. Ge, F. Shen, X.-Y. Jing, F. Wu, S.-P. Xie, D. Yue, and H.-B. Li, “Active contour evolved by joint probability classification on riemannian manifold,” *Signal, Image and Video Processing*, pp. 1–8, 2016.
- [11] S. Dai, H. Man, and S. Zhan, “Minimum mutual information based level set clustering algorithm for fast mri tissue segmentation,” in *2015 37th Annual International Conference of the IEEE Engineering in Medicine and Biology Society (EMBC)*. IEEE, 2015, pp. 3057–3060.
- [12] C. Li, J. C. Gore, and C. Davatzikos, “Multiplicative intrinsic component optimization (mico) for mri bias field estimation and tissue segmentation,” *Magnetic resonance imaging*, vol. 32, no. 7, pp. 913–923, 2014.
- [13] S. Osher and R. Fedkiw, *Level set methods and dynamic implicit surfaces*. Springer Science & Business Media, 2006, vol. 153.
- [14] G. Aubert and P. Kornprobst, *Mathematical problems in image processing: partial differential equations and the calculus of variations*. Springer Science & Business Media, 2006, vol. 147.
- [15] N. Houhou, J.-P. Thiran, and X. Bresson, “Fast texture segmentation model based on the shape operator and active contour,” in *Computer Vision and Pattern Recognition, 2008. CVPR 2008. IEEE Conference on*. IEEE, 2008, pp. 1–8.
- [16] K. Zhang, L. Zhang, H. Song, and D. Zhang, “Reinitialization-free level set evolution via reaction diffusion,” *IEEE Transactions on Image Processing*, vol. 22, no. 1, pp. 258–271, 2013.
- [17] X. Bresson, X.-C. Tai, T. F. Chan, and A. Szelam, “Multi-class transductive learning based on l1 relaxations of cheeger cut and mumford-shah-potts model,” *Journal of mathematical imaging and vision*, vol. 49, no. 1, pp. 191–201, 2014.
- [18] I. Endres and D. Hoiem, “Category independent object proposals,” in *European Conference on Computer Vision*. Springer, 2010, pp. 575–588.
- [19] P. Krähenbühl and V. Koltun, “Geodesic object proposals,” in *European Conference on Computer Vision*. Springer, 2014, pp. 725–739.
- [20] G. K. Douce, D. J. Moorhead, and C. T. BARGERON IV, “Forestry images. org: High resolution image archive and web-available image system,” *Journal of Forest Science*, vol. 47, pp. 77–79, 2001.